Redundant MEMS-based Inertial Navigation using Nonlinear Observers

Robert. H. Rogne
Department of Engineering Cybernetics,
Centre for Autonomous Marine Operations
and Systems (NTNU AMOS),
Norwegian University of Science
and Technology,
N-7491 Trondheim, Norway
Email: robert.rogne@ntnu.no

Torleiv. H. Bryne
Department of Engineering Cybernetics,
Centre for Autonomous Marine Operations
and Systems (NTNU AMOS),
Norwegian University of Science
and Technology,
N-7491 Trondheim, Norway
Email: torleiv.h.bryne@ntnu.no

Thor. I. Fossen
Department of Engineering Cybernetics,
Centre for Autonomous Marine
Operations and Systems (NTNU AMOS),
Norwegian University of Science
and Technology,
N-7491 Trondheim, Norway
Email: thor.fossen@ntnu.no

Tor. A. Johansen
Department of Engineering Cybernetics,
Centre for Autonomous Marine Operations
and Systems (NTNU AMOS),
Norwegian University of Science
and Technology,
N-7491 Trondheim, Norway
Email: tor.arne.johansen@ntnu.no

ABSTRACT

We present two alternative methods for fault detection and isolation (FDI) with redundant MEMS inertial measurement units (IMUs) in inertial navigation systems (INS) based on nonlinear observers. The first alternative is based on the parity space method, while the second is expanded with quaternion-based averaging and FDI. Both alternatives are implemented and validated using data gathered in a full-scale experiment on an offshore vessel. Data from three identical MEMS IMUs and the vessel's own industrial sensors is used to verify the methods' FDI capabilities. The results reveal that when it comes to FDI of the IMUs' angular rate sensors, there are differences

between the two methods. The navigation algorithm based on quaternion weighting is essentially unaffected by the failure of an angular rate sensor, while the parity-space-method-based alternative experiences a perturbation.

Nomenclature

$\{b\}$ BODY coordinate frame
$\{t\}$ Earth fixed tangent frame
$\{e\}$ Earth Centered Earth Fixed (ECEF) coordinate frame
$\{i\}$ Earth Centered Inertial (ECI) coordinate frame
R_b^t Rotation matrix from frame $\{b\}$ to frame $\{t\}$
q_b^t Unit quaternion representation of rotation from $\{b\}$ to $\{t\}$
ω_{ib}^b Angular velocity of $\{b\}$ relative $\{i\}$, decomposed in $\{b\}$
f_{ib}^t Specific force of $\{b\}$ decomposed in $\{t\}$
p_{tb}^t Position of $\{b\}$ relative $\{t\}$ decomposed in $\{t\}$
v_{tb}^t Velocity of $\{b\}$ relative $\{t\}$ decomposed in $\{t\}$
ϕ, θ, ψ Euler angles: Roll, pitch, yaw
μ Latitude
λ Longitude
$S(\cdot)$ Skew symmetric matrix such that $S(z_1)z_2 = z_1 \times z_2$
$\|\cdot\|_2$ Euclidean vector norm
I_n $n \times n$ identity matrix
$\otimes$ Hamiltonian quaternion product
TMO Translational motion observer
NLO Nonlinear observer
FDI Fault detection and isolation
MEMS Microelectromechanical system
IMU Inertial measurement unit
INS Inertial navigation system

1 Introduction

MEMS inertial sensors have gone through a substantial development during the last decades, [1], with increasing performance and lower cost. The advancement of MEMS IMUs has motivated research on nonlinear attitude observers such as [2–11]. Nonlinear observers (NLOs) have the benefit of explicit stability properties guaranteeing robustness. Similar properties are difficult to obtain with attitude estimators based on the extended Kalman filter (EKF) [12, 13] or the multiplicative EKF such as [14]. Another potential upside of using NLOs is that the attitude is estimated without propagating Riccati equations, therefore having a low computational footprint. Nonlinear observers for attitude estimation have also been integrated with position and velocity sensors resulting in a complete aided INS, [7].

For fault detection and isolation in inertial sensors, a method based on the generalized likelihood ratio test, [15], has prevailed for decades. The ratio is based on the likelihood given that the data fits either the main hypothesis H_0 (non-faulty) or under the alternative hypothesis H_1 (faulty data). For inertial sensors, the classical discrete methods [16, 17], and the continuous [18], employ parity equations to generate residuals for FDI. The inaccuracies of MEMS IMUs is a challenge when applying classical methods, [19, 20], so [19] proposed an improved method based on Mahalanobis distance. In [21], a Kalman filter with direction cosines was used to detect faults in a single MEMS IMU configuration for attitude determination. [22] uses four low-cost accelerometers and gyros in a truncated tethrahedon design with an information filter. In [23], an aircraft dynamic model is used together with the interacting multiple model and the unscented Kalman filter to improve state estimates in the face of inertial sensor faults. [24] provides a method for navigation sensor fault detection for a ground vehicle, using structural analysis. For the more generic case, [25] uses an intelligent particle filter for fault detection in nonlinear systems. In [26, 27], nonlinear observers are used for fault detection of navigation sensors on ships, but FDI was only applied to the aiding sensors, such as position references. The fault detection of inertial sensors should be done independently of aiding sensors, in order to avoid circular dependencies.

Redundant IMUs have traditionally been applied in safety-critical systems such as aircraft and spacecraft. In the maritime domain, dynamic positioning vessels are required to have redundant sensors on board. As for autonomous vehicles, in order for them to operate safely and autonomously, they need functions for self-diagnostics and fault management. To be feasible in the nascent consumer and commercial markets, it is not viable to fit these vehicles with high-end IMUs. Therefore, an investigation on how to improve the FDI performance with redundant MEMS sensors is of interest in the context of robust and low-complexity nonlinear observer-based INSs.

1.1 Main Contributions and Organization

The main contributions of this paper are

- Providing and comparing methods for fusing redundant MEMS inertial measurements using nonlinear attitude observers.
- Full-scale verification, using data collected from three MEMS IMUs mounted on an offshore vessel.

The paper is organized as follows: First the applied kinematic and sensors models are presented, before the observers used throughout the paper are introduced. Thereafter, a full-scale verification is performed with a subsequent discussion. Finally, the paper is concluded.

2 Preliminaries

2.1 Kinematic Strapdown Equations

The most intuitive attitude representation of a vessel is between the BODY and a North-East-Down or a tangent frame. For navigation of craft confined to a specific geographical area, the fixed tangent frame is a suitable navigation frame. The kinematic attitude strapdown equation between the BODY and the tangent frame becomes

$$\dot{q}_b^t = \frac{1}{2} q_b^t \otimes \begin{pmatrix} 0 \\ \omega_{ib}^b \end{pmatrix} - \frac{1}{2} \begin{pmatrix} 0 \\ \omega_{it}^t \end{pmatrix} \otimes q_b^t, \tag{1}$$

where

$$\omega_{it}^t = \omega_{ie}^t + \omega_{et}^t = \omega_{ie}^t, \tag{2}$$

because $\omega_{et}^t = 0_{3\times 1}$ since the tangent frame is Earth fixed. ω_{ib}^b is the angular rate of the vehicle relative the inertial frame $\{b\}$. When using $\{t\}$ as the navigation frame, the rotational and translational motion has the relationship [12],

$$\dot{p}_{tb}^t = v_{tb}^t, \tag{3}$$

$$\dot{v}_{tb}^t = -2S(\omega_{ie}^t) v_{tb}^t + R_b^t f_{ib}^b + g_b^t, \tag{4}$$

where $R_b^t = R(q_b^t) = I_3 + 2sS(r) + 2S^2(r)$, $p_{tb}^t \in \mathbb{R}^3$ is the position relative the origin of the tangent frame, and $v_{tb}^t \in \mathbb{R}^3$ is the linear velocity. $g_b^t(\mu, \lambda) \in \mathbb{R}^3$ is the local gravity vector. $f_{ib}^b = (R_b^t)^\intercal (a_{ib}^t - g_b^t) \in \mathbb{R}^3$ is the specific force, measured by the IMU, where a_{ib}^t represents the crafts accelerations in the tangent frame.

2.2 Inertial and Heading Sensors

An IMU triad comprises sensors along three orthogonal axes, measuring angular rate and specific force. Each of the measurements are contaminated with noise and biases and potentially faults. For the sensor outputs, we have the following model:

$$\omega_{\text{IMU}}^b = \omega_{ib}^b + b_{\text{gyro}}^b + w_{\text{gyro}}^b + d_{\text{gyro}}^b, \tag{5}$$

$$f_{\text{IMU}}^b = f_{ib}^b + b_{\text{acc}}^b + w_{\text{acc}}^b + d_{\text{acc}}^b \tag{6}$$

where, in addition to the true angular rates and specific forces, b_{gyro}^b and b_{acc}^b are the biases, while w_{gyro}^b and w_{acc}^b represent sensor noise. $d_\star^b$ denotes sensor faults. Both the angular rate and accelerometer biases are assumed to be slowly time-varying. In addition to the IMU, we assume that a heading reference ψ_{ref} is available.

3 Nonlinear Observer Structure

3.1 Observer Structures for fusing redundant measurements

We will compare two different structures applicable for redundant IMU FDI. In alternative 1 the gyro and accelerometer outputs from the IMUs are combined into single measurements via the parity space method. In alternative 2 (Fig. 1), only the accelerometer measurements are combined beforehand, while the angular rate measurements are sent to three instances of a nonlinear observer. The outputs of these observers are then merged and forwarded to an aiding TMO. While we employ a specific nonlinear attitude observer, the results are not inherently dependent on the INS implementation because of the methods' modular nature.

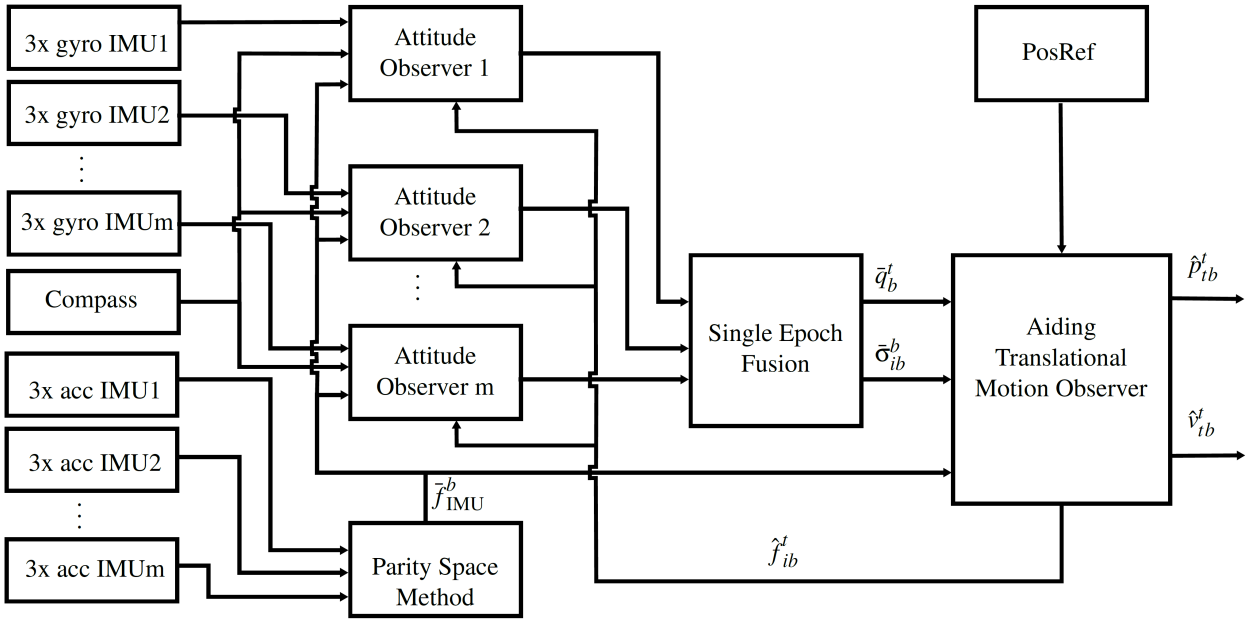

Fig. 1. Redundant IMU alternative 2 – Observer structure.

3.2 Attitude Observer

The attitude observer instances are based on the NLO found in [28]:

$$\Sigma_{1,j}: \begin{cases} \dot{\hat{q}}^t_{b,j} = \frac{1}{2}\hat{q}^t_{b,j} \otimes \begin{pmatrix} 0 \\ \hat{\omega}^b_{ib,j} \end{pmatrix} - \frac{1}{2}\begin{pmatrix} 0 \\ \omega^t_{it} \end{pmatrix} \otimes \hat{q}^t_{b,j}, & (7a) \\ \hat{\omega}^b_{ib,j} = \omega^b_{\text{IMU},j} - \hat{b}^b_{\text{gyro},j} + \hat{\sigma}^b_{ib,j}, & (7b) \\ \dot{\hat{b}}^b_{\text{gyro},j} = \text{Proj}\left(\hat{b}^b_{\text{gyro},j}, -k_I \hat{\sigma}^b_{ib,j}\right), & (7c) \end{cases}$$

where

$$\hat{\sigma}^b_{ib,j} = k_1 \underline{v}^b_1 \times R^\intercal(\hat{q}^t_{b,j})\underline{v}^t_1 + k_2 \underline{v}^b_2 \times R^\intercal(\hat{q}^t_{b,j})\underline{v}^t_2. \tag{8}$$

$\text{Proj}(\cdot,\cdot)$ denotes a projection algorithm [7], imposing a bound on $\hat{b}^b_{\text{gyro},j}$ to a compact set. k_1, k_2 and k_I are observer gains. The observers are implemented with the injection terms, $\hat{\sigma}^b_{ib,j}$, where the j^{th} observer uses its own attitude estimate $\hat{q}^t_{b,j}$, and the reference vectors

$$\begin{aligned} \underline{v}^b_1 &= \underline{f}^b_{ib}, \quad \underline{v}^b_2 = \underline{f}^b_{ib} \times \underline{c}^b_{tb}, \\ \underline{v}^t_1 &= \underline{f}^t_{ib}, \quad \underline{v}^t_2 = \underline{f}^t_{ib} \times \underline{c}^t_{tb}. \end{aligned}$$

where

$$\underline{f}^b_{ib} = \frac{\bar{f}^b_{\text{IMU}}}{\|\bar{f}^b_{\text{IMU}}\|_2}, \tag{9}$$

$$\underline{c}^b_{tb} = \left(\cos(\psi_{\text{ref}}), -\sin(\psi_{\text{ref}}), 0\right)^\intercal, \tag{10}$$

$$\underline{f}^t_{ib} = \frac{\text{sat}_{M_f}(\hat{f}^t_{ib})}{\|\text{sat}_{M_f}(\hat{f}^t_{ib})\|_2}, \tag{11}$$

$$\underline{c}^t_{tb} = \left(1, 0, 0\right)^\intercal, \tag{12}$$

and $\bar{f}^b_{\text{IMU}}$ is the fused accelerometer signal, see Sec. 4.

3.3 Translational Motion Observer

The translational motion observer (TMO) estimates position, linear velocity and specific forces $\hat{p}^t_{tb} \in \mathbb{R}^3$, $\hat{v}^t_{tb} \in \mathbb{R}^3$ and $\hat{f}^t_{tb} \in \mathbb{R}^3$, in the given navigation frame $\{t\}$. The resulting TMO takes the form,

$$\Sigma_2 : \begin{cases} \dot{\hat{p}}^t_{tb} = \hat{v}^t_{tb} + \theta K_{pp} \tilde{p}^t_{tb} & \text{(13a)} \\ \dot{\hat{v}}^t_{tb} = -2S(\omega^t_{ie})\hat{v}^t_{tb} + \hat{f}^t_{ib} + g^t_b + \theta^2 K_{vp} \tilde{p}^t_{tb} & \text{(13b)} \\ \dot{\xi}^t_{ib} = -R\left(\bar{q}^t_b\right) S\left(\bar{\sigma}^b_{ib}\right) \bar{f}^b_{\text{IMU}} + \theta^3 K_{\xi p} \tilde{p}^t_{tb} & \text{(13c)} \\ \hat{f}^t_{ib} = R\left(\bar{q}^t_b\right) \bar{f}^b_{\text{IMU}} + \xi^t_{ib}, & \text{(13d)} \end{cases}$$

where θ is a high-gain parameter, $K_{\star\star}$ are gain matrices and $\tilde{p}^t_{tb}$ is position error. ξ^t_{ib} is an intermediary parameter. The estimator is equivalent to the design of [28] except for use of the tangent frame $\{t\}$ instead of the ECEF frame $\{e\}$ as navigation frame, and the use of fused signals $\bar{f}^b_{\text{IMU}}$, $\bar{q}^t_b$ and $\bar{\sigma}^b_{ib}$ based on the signals $f^b_{\text{IMU},j}$, $\hat{q}^t_{b,j}$ and $\hat{\sigma}^b_{ib,j}$.

4 Parity Space Method

In the parity space method [17], the detection of faults comes down to a statistical test, based on a decision variable obtained from separating the measurement space, i.e. all the redundant measurements, into two subspaces: the parity space and the dimensional state space, where the latter is essentially the vehicle's BODY frame.

For $l = 3m$ measurements of a 3-dimensional state vector x, we have the measurement model

$$y^b_{\text{IMU}} = H x^b_{ib} + w^b_\star + b^b_\star + d^b_\star \tag{14}$$

where $H = (I_3, I_3, \ldots, I_3)^\intercal$ is the measurement matrix relating the state space to the measurement space, and x^b_{ib} is the state space value of interest, in this case either ω^b_{ib} or f^b_{ib} as described in Section 2.2. Then, the least squares estimate of x^b_{ib} in (14) simply becomes

$$\bar{x}^b_{ib} = (H^\intercal H)^{-1} H^\intercal y^b_{\text{IMU}}. \tag{15}$$

For details on fault detection and isolation with the parity space method, the reader is referred to [17] or [19].

5 Quaternion Averaging and FDI

The estimated unit quaternions from Sec. 3.2 ($\hat{q}^t_{b,1}, \hat{q}^t_{b,2}, \ldots, \hat{q}^t_{b,m}$) can be weighed optimally using a single epoch estimation algorithm, such as in [29]. Standard averaging will not maintain the unit quaternions' properties because of the attitude's topological $SO(3)$ constraints, [30].

For the detection and isolation of faults in quaternions, we employ the angle between orientations represented by the unit quaternions. The unit quaternion conjugate of q is defined $(q)^* := (s, -r^\intercal)^\intercal$. The error quaternion between two unit quaternions q and p is defined as $\tilde{q} := q \otimes p^*$. The scalar part of the error quaternion $\tilde{q}$ can be calculated by

$$\tilde{s} = q_1 p_1 + q_2 p_2 + q_3 p_3 + q_4 p_4, \tag{16}$$

which is equal to $q^\intercal p$. Now, consider that $\tilde{\beta}$ is the angle of rotation represented by the error quaternion about some axis, and consequently, a measure of the error's magnitude. Then, the relationship between the scalar part and the angle is given as [31],

$$\begin{aligned} \tilde{s} &:= \cos\left(\frac{\tilde{\beta}}{2}\right) \\ \implies \tilde{\beta} &= 2\arccos(\tilde{s}) \\ \implies \tilde{\beta} &= 2\arccos(q^\intercal p). \end{aligned} \tag{17}$$

ALGORITHM 1. Quaternion FDI

Require: $\hat{q}^t_{b,1} \dots \hat{q}^t_{b,m}$, α_{det}
  b_dont_stop = true
  while b_dont_stop **do**
    $\bar{q}^t_b = \text{quat\_avg}(\hat{q}^t_{b,j} \dots \hat{q}^t_{b,m})$
    for $j = 1$ **to** m **do**
      $\tilde{\beta}_j = 2\arccos\left(|(\hat{q}^t_{b,j})^\intercal \bar{q}^t_b|\right)$
    end for
    if $\text{any}(\tilde{\beta}_j) > \alpha_{det}$ **then**
      $k = \arg\max_{j\in[1;m]} \tilde{\beta}_j$
      Remove quaternion, $\hat{q}^t_{b,k}$
    else
      b_dont_stop = false
    end if
  end while
Output: $\bar{q}^t_b$

Equation (17) may serve as a useful metric for FDI. However, for $\rho \in [0, 1]$, due to

$$\beta = 2\arccos(\rho) = 2\pi - 2\arccos(-\rho), \tag{18}$$

and the fact that q and $-q$ represents the same rotation, we can instead use the absolute value of the dot product to avoid calculating the absolute error angle. Therefore,

$$\tilde{\beta}_j = 2\arccos\left(|(\hat{q}^t_{b,j})^\intercal \bar{q}^t_b|\right), \tag{19}$$

is chosen as detection variable. If any of the $\tilde{\beta}_j$ values are over a given threshold α_{det}, quaternion j is removed from the average. See Algorithm 1 for details. The threshold α_{det} is chosen as the maximum allowable angle difference between the j^{th} quaternion estimate and the average. In order to minimize the rate of false alarms, a lower bound on α_{det} could be determined by using empirical data from a fault-free case.

The injection term $\hat{\sigma}^b_{ib,j} \in \mathbb{R}^3$ may evolve freely on $\mathbb{R}^3$ with no topological constraints. Thus, the fused injection term, $\bar{\sigma}^b_{ib}$ is obtained with least-squares-based weighting.

6 Case Study

In this section we present a case study for redundant IMUs onboard an offshore vessel operation in the Norwegian sea. A modified version of the translational motion observer in Section 3.3 is employed, developed for surface vessels and heave estimation, [32]. Regarding the sensor configuration, three ADIS16485 MEMS IMUs were installed. The vessel's industrial vertical reference units, GNSS and gyrocompasses were used for comparison, and the two latter for aiding as well. The details of these sensors can be found in [33]. The vessel was doing a dynamic positioning operation at the time of data collection.

6.1 Full-scale testing for FDI

For fault injection, we used a fault free dataset and added artificial faults to the accelerometer and angular rate sensor.

6.1.1 Accelerometer fault

A bias of 1 m/s^2 is added to the x-axis of ADIS2 at $t = 20$min. Fig. 2 shows the fault detection variables and the fault status of the accelerometer. The faulty sensor is removed in an orderly fashion, resulting in practically no effect on the estimates.

6.1.2 Angular rate sensor fault

For ADIS3, the gyro bias is increased by 1 deg/s on the y-axis at $t = 20$min. For Alternative 1, we observe from Fig. 3 that the attitude estimates deviate when the fault occurs, before converging back to zero estimation error.

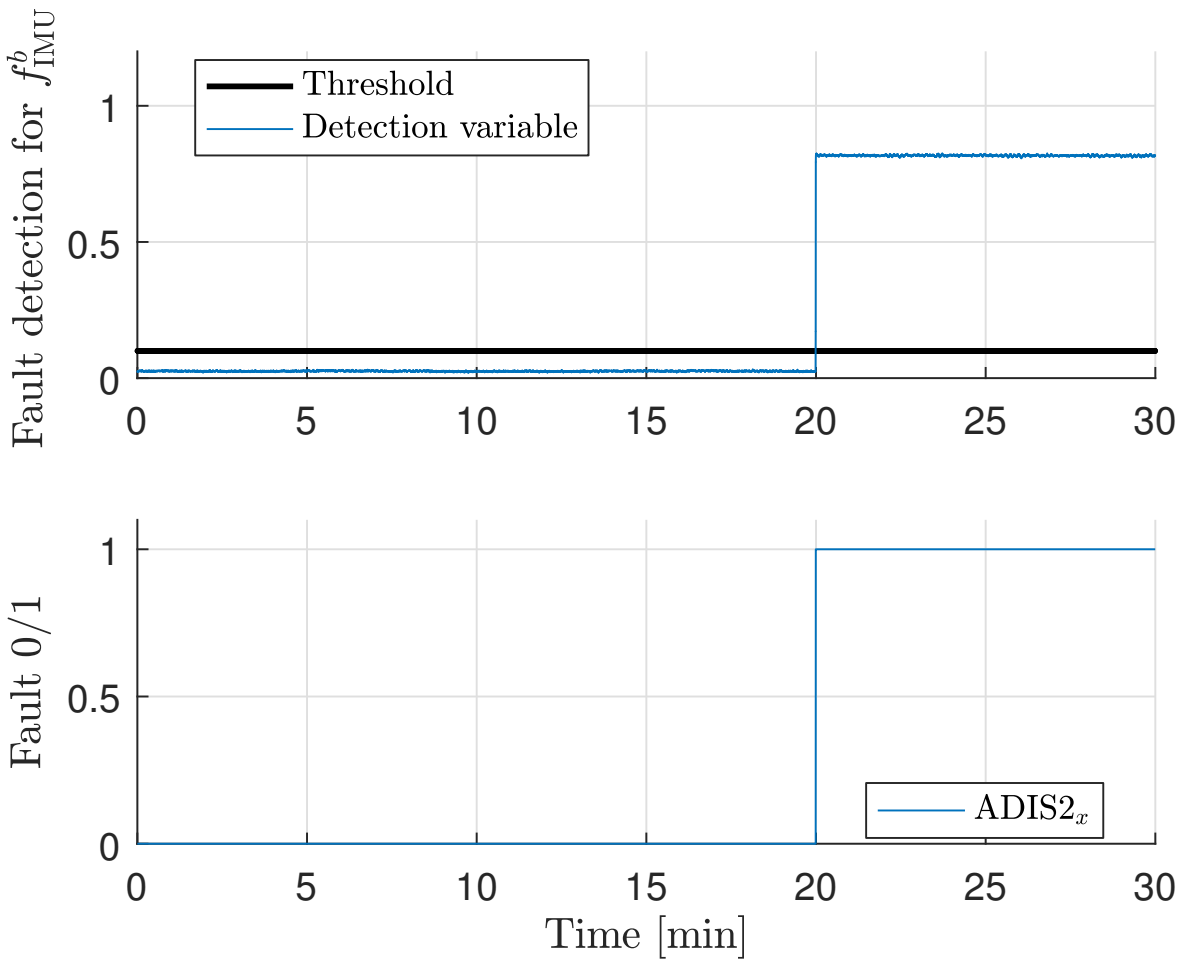

Fig. 2. Fault detection for accelerometer fault. Parity space method.

From Fig. 5 we learn that the averaged attitude estimates of Alternative 2 are not significantly affected by the fault, while the one faulty estimator remains erroneous. Fig. 6 shows the FDI at work. When fault occurs at $t = 20$min, it is properly detected and isolated, and the faulty estimator output is removed from the quaternion average.

6.2 Discussion

FDI for the accelerometer with the parity space method proved successful. For the angular rate sensors however, a problem arose as shown in Fig. 7. In the parity space method, all three IMUs are merged and treated as one, which means that the bias of the merged IMU output is the average of three IMUs. When removing a sensor, the average bias estimate is shifted, causing a perturbation in the attitude estimate (Fig. 3), while the nonlinear observer re-estimates the new bias. The quaternion-based FDI algorithm fared better in this concern, quickly voting out the erroneous estimator. On the other hand, after the estimate of Alternative 1 has converged again this method has the advantage, seeing as eight gyro axes are still in play versus only six in Alternative 2, since a whole gyro triad providing input to the faulty observer is removed.

7 Summary

Two alternatives for FDI with redundant MEMS IMUs using nonlinear observers has been presented. One alternative was based on the classic parity space method, while the other also employed a quaternion-based averaging, fault detection and fault isolation scheme. The structural differences between the alternatives were layed out, and we developed algorithms for both. The algorithms were validated on full-scale experimental data acquired from an offshore vessel, using three ADIS16485 IMUs. In addition, we also used the ship's industry-proven gyrocompass and vertical reference units for comparison.

Artificial faults were injected into the measurement signals for FDI. In the accelerometer fault case, the fault was detected and isolated rapidly, and the FDI in this case was purely based on the parity space method in both alternatives. For the angular rate sensor fault, the parity space method implemented here showed some weaknesses compared to the

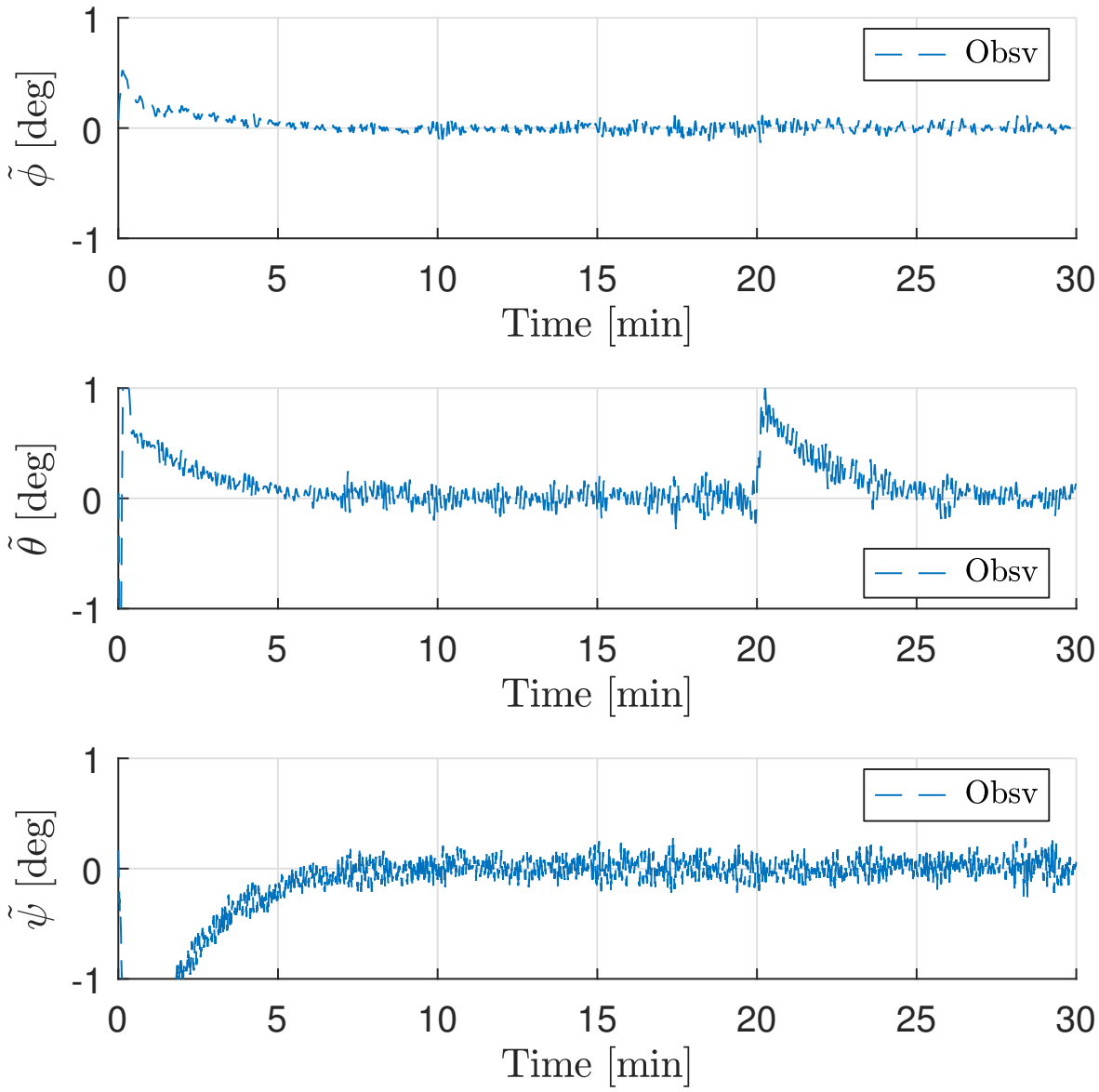

Fig. 3. Attitude estimation error. Parity space method for angular rate sensor (Alternative 1).

quaternion-based method, but both methods successfully detected and isolated the fault.

Acknowledgements

This work has been carried out at the Centre for Autonomous Marine Operations and Systems (NTNU AMOS) and supported by the Research Council of Norway and Rolls–Royce Marine through the Centres of Excellence funding scheme and the MAROFF programme, grant numbers 223254 and 225259. The Research Council of Norway is acknowledged as the main sponsor of NTNU AMOS.

The authors wish to thank the mechanical and electronics workshop at the Department of Engineering Cybernetics, Rolls-Royce Marine and Farstad Shipping for assistance in the process of developing and installing the sensor payload on board the offshore vessel.

References

[1] Barbour, N., Hopkins, R., and Kourepenis, A., 2011. Inertial MEMS system applications. Tech. rep., NATO Lecture series RTO-EN-SET-116 Low-Cost Navigation Sensors and Integration Technology, March.

[2] Salcudean, S., 1991. "A globally convergent angular velocity observer for rigid body motion". *IEEE Trans. Automat. Contr.,* **36**(12), pp. 1493 – 1497.

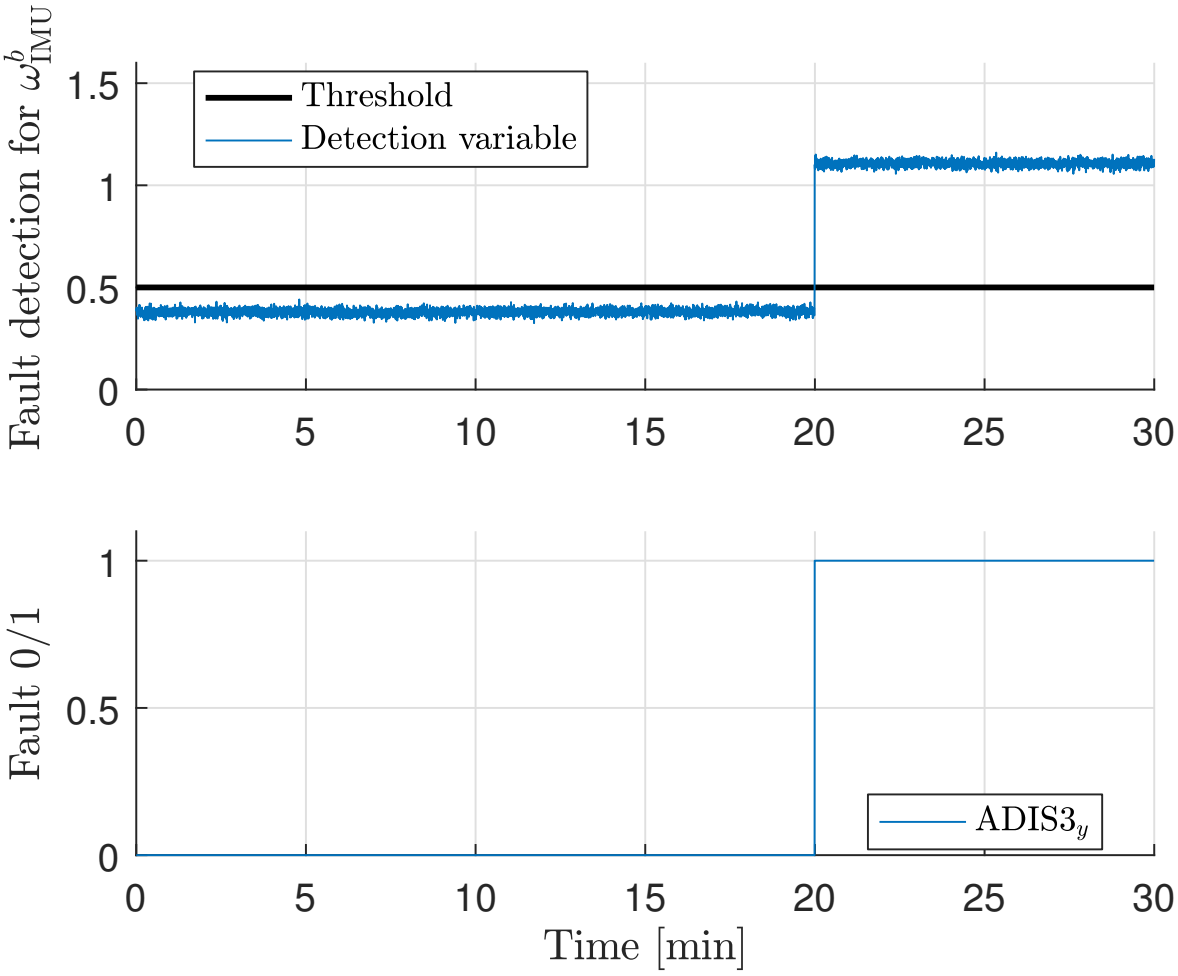

Fig. 4. Fault detection for angular rate sensor fault. Parity space method (Alternative 1).

[3] Vik, B., and Fossen, T., 2001. "A nonlinear observer for GPS and INS integration". In Proc. IEEE Conf. Dec. Cont, Vol. 3, pp. 2956–61.

[4] Mahony, R., Hamel, T., and Pflimlin, J. M., 2008. "Nonlinear complementary filters on the special orthogonal group". *IEEE Transactions on Automatic Control,* **53**(5), pp. 1203–2018.

[5] Martin, P., and Salaün, E., 2010. "Design and implementation of a low-cost observer-based attitude and heading reference system". *Control Engineering Practice,* **18**(7), pp. 712—722.

[6] Hua, M.-D., 2010. "Attitude estimation for accelerated vehicles using GPS/INS measurements". *Control Engineering Practice,* **18**(7), pp. 723–732.

[7] Grip, H. F., Fossen, T. I., Johansen, T. A., and Saberi, A., 2012. "Attitude estimation using biased gyro and vector measurements with time-varying reference vectors". *IEEE Transactions on Automatic Control,* **57**(5), pp. 1332—1338.

[8] Batista, P., Silvestre, C., and Oliveira, P., 2012. "A GES attitude observer with single vector observations". *Automatica,* **48**(2), pp. 388–39.

[9] Batista, P., Silvestre, C., and Oliveira, P., 2012. "Globally exponentially stable cascade observers for attitude estimation". *Control Engineering Practice,* **20**(2), pp. 148–155.

[10] Hua, M.-D., Ducard, G., Hamel, T., Mahony, R., and Rudin, K., 2014. "Implementation of a nonlinear attitude estimator for aerial robotic vehicles". *IEEE Transactions On Control System Technology,* **22**(1), pp. 201–212.

[11] Hua, M.-D., Martin, P., and Hamel, T., 2016. "Stability analysis of velocity-aided attitude observers for accelerated vehicles". *Automatica,* **63**, pp. 11–15.

[12] Farrell, J. A., 2008. *Aided Navigation: GPS with High Rate Sensors*. McGraw-Hill.

[13] Groves, P. D., 2013. *Principles of GNSS, Inertial, and Multisensor Integrated Navigation Systems*, 2nd ed. Artech House.

[14] Markley, F. L., 2003. "Attitude error representation for kalman filtering". *Journal of Guidance, Control and Dynamics,* **26**(2), March, pp. 311–317.

[15] Willsky, A., and Jones, H., 1976. "A generalized likelihood ratio approach to the detection and estimation of jumps in

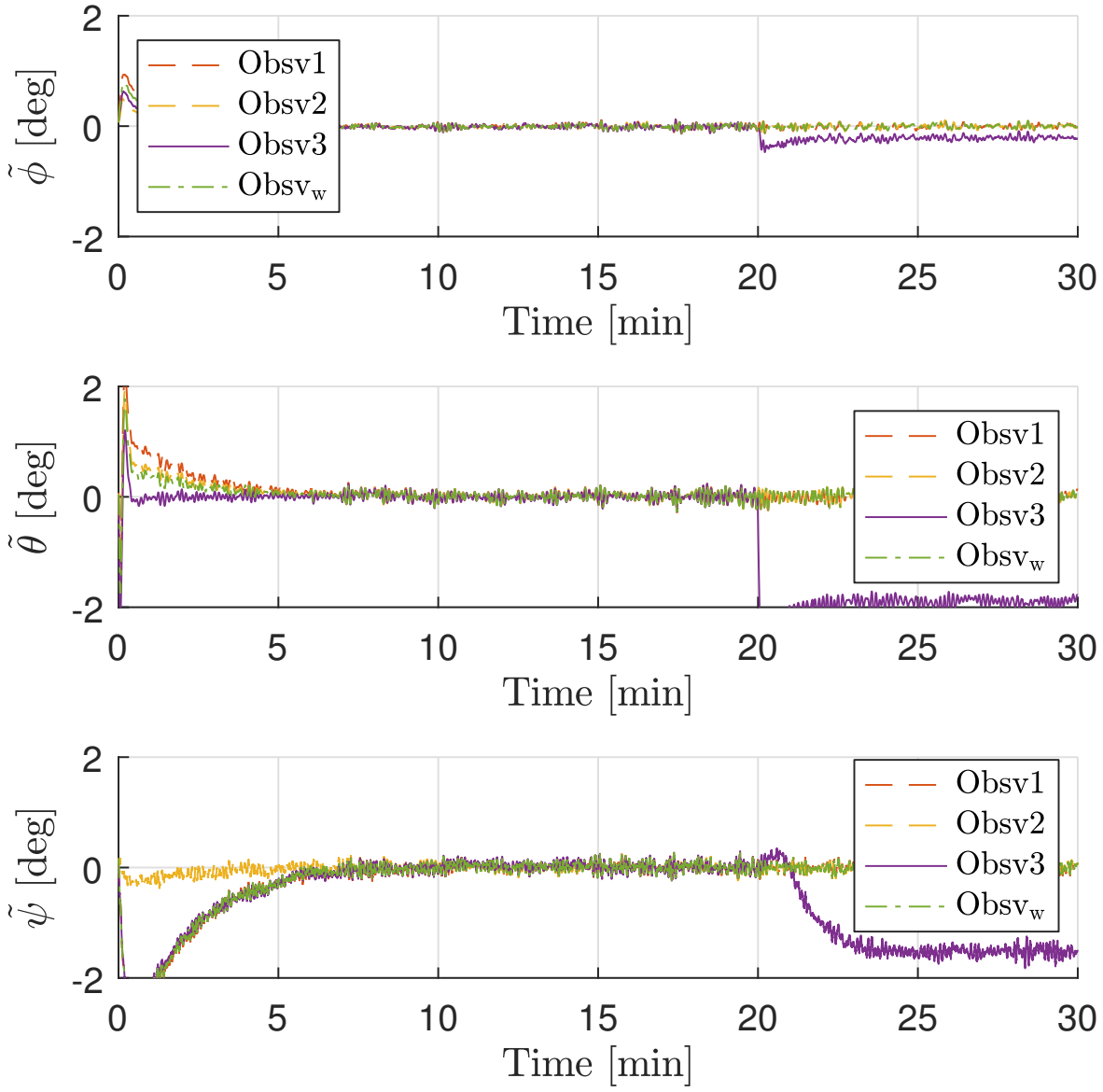

Fig. 5. Attitude estimation error. Quaternion FDI method angular rate sensor (Alternative 2).

linear systems". *IEEE Transactions on Automatic control,* **21**(1), pp. 108–112.

[16] Daly, K. C., Gai, E., and Harrison, J. V., 1979. "Generalized likelihood test for FDI in redundant sensor configurations". *Journal of Guidance, Control, and Dynamics,* **2**(1), pp. 9–17.

[17] Sturza, M. A., 1988. "Navigation system integrity monitoring using redundant measurements". *Navigation,* **35**(4), pp. 483–501.

[18] Medvedev, A., 1995. "Fault detection and isolation by a continuous parity space method". *Automatica,* **31**(7), pp. 1039–1044.

[19] Guerrier, S., Waegli, A., Skaloud, J., and Victoria-Feser, M.-P., 2012. "Fault detection and isolation in multiple mems-imus configurations". *IEEE Transactions on Aerospace and Electronic Systems,* **48**(3), pp. 2015–2031.

[20] Waegli, A., Guerrier, S., and Skaloud, J., 2008. "Redundant MEMS-IMU integrated with GPS for performance assessment in sports". In 2008 IEEE/ION Position, Location and Navigation Symposium, IEEE, pp. 1260–1268.

[21] Carminati, M., Ferrari, G., Grassetti, R., and Sampietro, M., 2012. "Real-time data fusion and mems sensors fault detection in an aircraft emergency attitude unit based on kalman filtering". *IEEE sensors journal,* **12**(10), pp. 2984–2992.

[22] Sukkarieh, S., Gibbens, P., Grocholsky, B., Willis, K., and Durrant-Whyte, H. F., 2000. "A low-cost, redundant inertial measurement unit for unmanned air vehicles". *The International Journal of Robotics Research,* **19**(11), pp. 1089–1103.

[23] Cork, L., and Walker, R., 2007. "Sensor fault detection for UAVs using a nonlinear dynamic model and the IMM-UKF

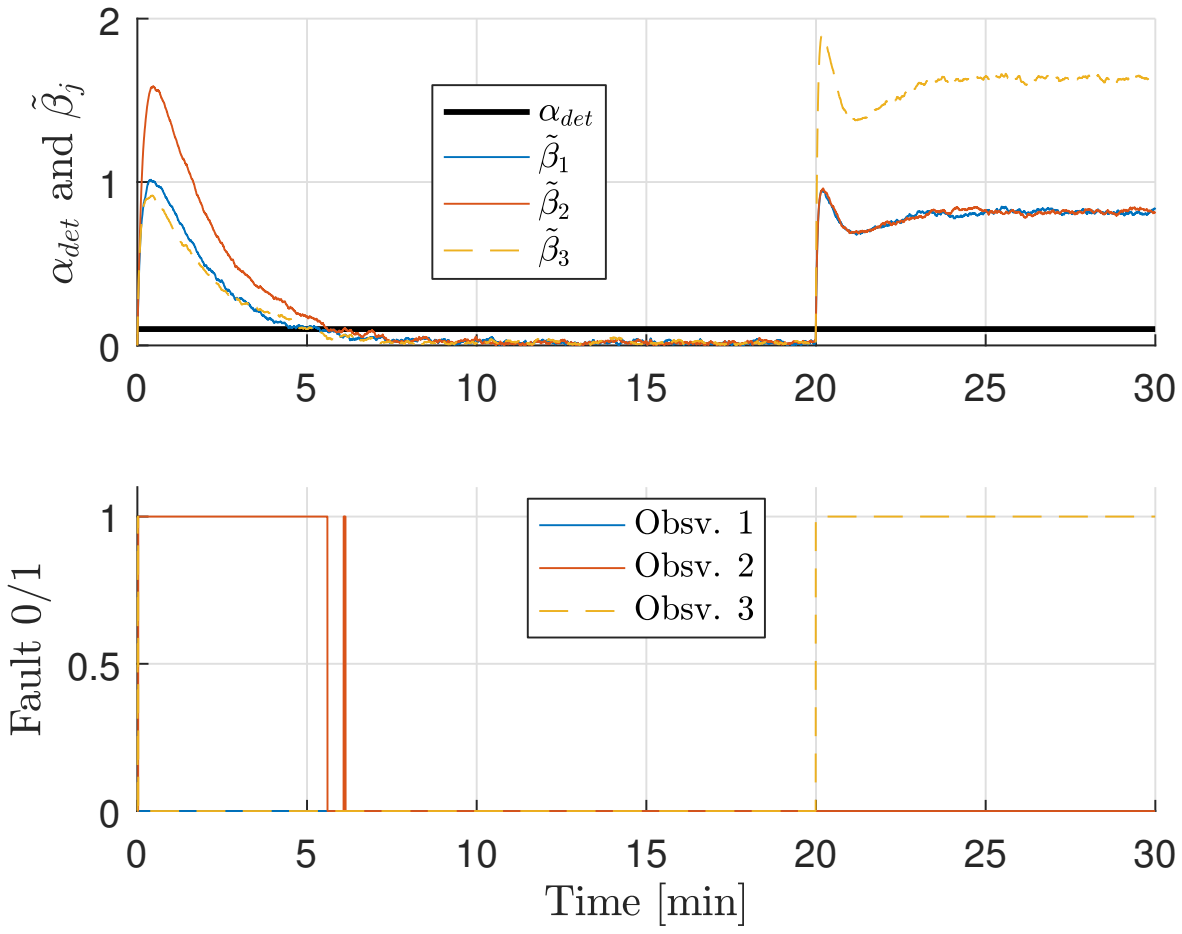

Fig. 6. Fault detection for angular rate sensor fault. Quaternion FDI (Alternative 2).

algorithm". In 2007 Information, Decision and Control, pp. 230–235.

[24] Monteriù, A., Asthana, P., Valavanis, K., and Longhi, S., 2007. "Residual generation approaches in navigation sensors fault detection applications". In 2007 European Control Conference (ECC), pp. 1022–1029.

[25] Yin, S., and Zhu, X., 2015. "Intelligent particle filter and its application to fault detection of nonlinear system". *IEEE Transactions on Industrial Electronics,* **62**(6), June, pp. 3852–3861.

[26] Rogne, R. H., Bryne, T. H., Johansen, T. A., and Fossen, T. I., 2016. "Fault detection in lever-arm-compensated position reference systems based on nonlinear attitude observers and inertial measurements in dynamic positioning". In Proc. of the American Contr. Conf., pp. 985–992.

[27] Bryne, T. H., Fossen, T. I., and Johansen, T. A., 2015. "Design of inertial navigation systems for marine craft with adaptive wave filtering aided by triple-redundant sensor packages". *International Journal of Adaptive Control and Signal Processing*, pp. 1–23.

[28] Grip, H. F., Fossen, T. I., Johansen, T. A., and Saberi, A., 2013. "Nonlinear observer for GNSS-aided inertial navigation with quaternion-based attitude estimation". In Proc. of the American Contr. Conf., pp. 272–279.

[29] Markley, F. L., 2007. "Averaging quaternions". *Journal of Guidance, Control and Dynamics,* **30**(4), pp. 1193–1196.

[30] Bhat, S., and Bernstein, D., 2000. "A topological obstruction to continuous global stabilization of rotational motion and the unwinding phenomenon". *Systems & Control Letters,* **39**(1), pp. 63–70.

[31] Chou, J. C., 1992. "Quaternion kinematic and dynamic differential equations". *IEEE Transactions on robotics and automation,* **8**(1), pp. 53–64.

[32] Bryne, T. H., Fossen, T. I., and Johansen, T. A., 2015. "A virtual vertical reference concept for GNSS/INS applications at the sea surface". In Proc. of the 10th IFAC Conference on Manoeuvring and Control of Marine Craft, pp. 127–133.

[33] Rogne, R. H., Bryne, T. H., Fossen, T. I., and Johansen, T. A., 2016. "MEMS-based inertial navigation on dynamically positioned ships: Dead reckoning". In Proc. of the 10th IFAC Conference on Control Applications in Marine Systems, pp. 139—146.

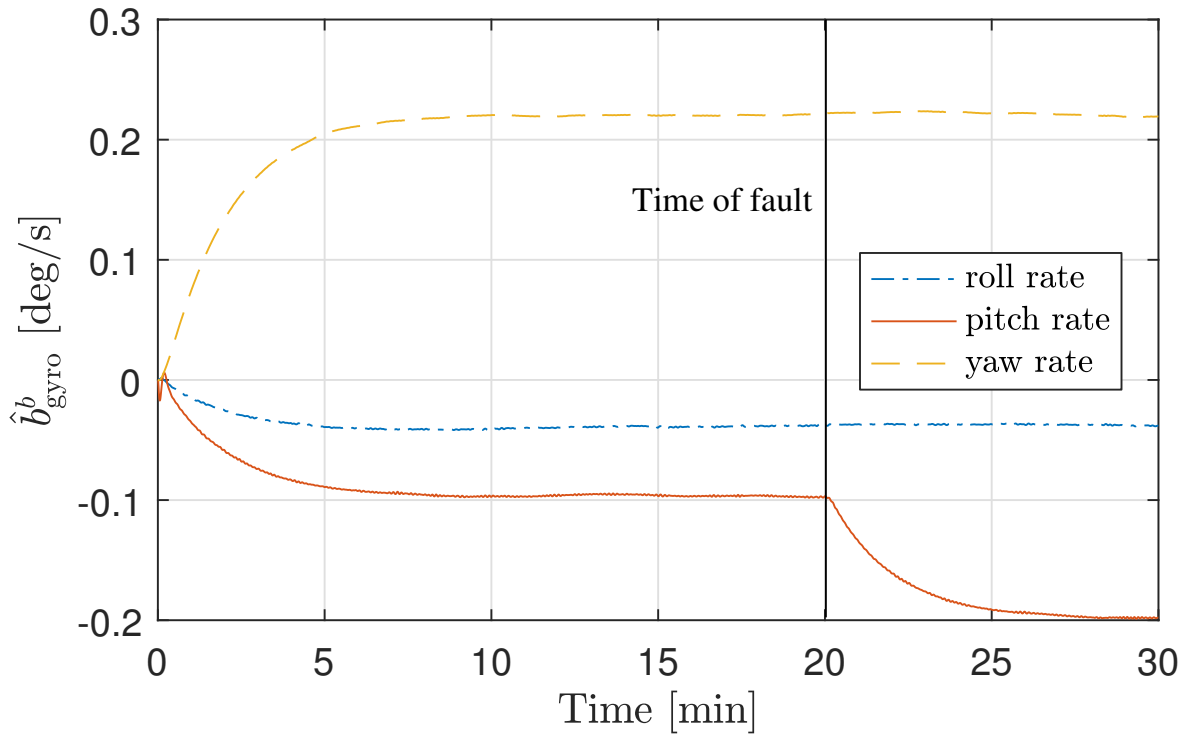

Fig. 7. Gyro bias estimates. Parity space method for angular rate sensor (Alternative 1).

List of Figures